The 14th World Conference on Earthquake Engineering
October 12-17, 2008, Beijing, China

Can Tsunami Drawdown Lead to Liquefaction Failure of Coastal Sandy Slopes?

Y.L. Young[1], H. Xiao[2], J.A. White[3], R.I. Borja[4]

[1] *UPS Visiting Professor, Dept. of Civil and Environmental Engineering, Stanford University, CA, USA*
Assistant Professor, Dept. of Civil and Environmental Engineering, Princeton University, NJ, USA
[2] *Graduate Student, Dept. of Civil and Environmental Engineering, Princeton University, NJ, USA*
[3] *Graduate Student, Dept. of Civil and Environmental Engineering, Stanford University, CA, USA*
[4] *Professor, Dept. of Civil and Environmental Engineering, Stanford University, CA, USA*

Email: yyoung@princeton.edu, xiao@princeton.edu, joshua.white@stanford.edu, borja@stanford.edu

ABSTRACT:

A significant tsunami can cause severe damage to coastlines and coastal structures due to inundation, erosion, as well as hydrodynamic and debris impact. However, although there exist many analytical, numerical, and experimental studies of tsunami wave propagation and inundation modeling, few studies considered the possibility of tsunami induced liquefaction failure of coastal sandy slopes. The objective of this work is to investigate the liquefaction potential of planar fine sand slopes during tsunami runup and drawdown. The transient pressure distribution acting on the slope due to wave runup and drawdown is computed by solving for the hybrid Boussinesq – nonlinear shallow water equations using a finite volume method. The subsurface pore water pressure distribution is solved using a finite element method. The numerical methods are validated by comparing the results with experimental measurements from a large-scale laboratory study of breaking solitary waves over a planar fine sand beach. Numerical predictions are shown for a 10m solitary wave over a 1:15 and 1:5 sloped fine sand beach. The results show that the soil near the bed surface along the seepage face created during the drawdown is subject to liquefaction failure.

1. INTRODUCTION

As demonstrated by the 2004 Indian Ocean Tsunami, high intensity wave runup and drawdown can cause significant loss of lives, as well as costly damages to coastlines and coastal structures. In addition to severe erosion and scour around coastal structures, liquefaction failure of coastal slopes may also develop. The rapid loading and unloading caused by wave runup and drawdown may generate high enough hydraulic gradients to fluidize the nearly saturated sandy deposit near the bed surface, leading to liquefaction failure of the coastal slopes. However, although there exist many analytical, numerical, and experimental studies of tsunami wave propagation and inundation modeling, few studies considered the effects of the mobile bed. Hence, the potential for tsunami induced liquefaction failure of coastal slopes has been mostly ignored.

Over the past few decades, there have been a significant number of studies related to wave-induced liquefaction failure of sandy seabed. An excellent review of work reported in the past 50 years has been presented in Jeng (2003). However, almost all past studies of wave-seabed interactions focused on pore water pressure fluctuations due to passing of wave crests and troughs over a flat seabed, and ignored the effects of wave runup and drawdown in the near-shore region. Moreover, most past studies focused on short-period wind generated waves, which are very different from tsunamis. A tsunami is characterized by a single or a few long period waves spaced far apart in time. The amplitude of a tsunami can easily exceed 10 m, the runup can reach miles on shore, and the drawdown can cause the water level to drop significantly below the initial water surface, exposing a large portion of the beach face that was previous submerged.

Currently, there are not enough quantitative laboratory or field data to examine the response of coastal slopes to transient loading and unloading due to tsunami runup and drawdown. This is due, in part, to the difficulty in obtaining real time data on site. Moreover, reconnaissance surveys can only provide very limited information about the sequence of events and actual failure mechanisms. Laboratory studies are also difficult to conduct and interpret due to scaling conflicts between the fluid and the porous media. Hence, numerical modeling is a valuable tool to study the response and failure mechanisms of coastal slopes subject to tsunami runup and drawdown.

The objective of this work is to develop and validate a numerical model to assess the potential for tsunami-induced liquefaction failure of coastal sandy slopes.

2. NUMERICAL MODEL

2.1 Surface Wave Simulator - FVM

To model the tsunami runup and drawdown, we solved the depth-averaged nonlinear shallow water equations (SWE) and Boussinesq equations. The nonlinear shallow water equations have been used by many authors (Wei et al. 2006; Kim et al. 2004; Zhang 1996) to investigate the propagation, runup, and drawdown of long-period waves. Since the dispersion effects are believed to be important before the wave-breaking, Boussinesq equations are solved during the pre-breaking phase, while the SWEs are solved post breaking. The switch to SWE after wave breaking is to avoid numerical instabilities caused by the high order terms from the dispersions. The governing equations are presented below, formulated after (Borthwick et al. 2005):

$$\frac{\partial \mathbf{U}^*}{\partial t} + \frac{\partial \mathbf{F}}{\partial x} = \mathbf{S} \tag{2.1}$$

where $\mathbf{U}^*$ is the vector of conservative variable

$$\mathbf{U}^* = \mathbf{U} + \begin{Bmatrix} 0 \\ \left(B + \frac{1}{3}\right) d^2 (hu)_{xx} + \frac{1}{3} d d_x (hu)_x \end{Bmatrix} \quad \text{and} \quad \mathbf{U} = \begin{Bmatrix} h \\ hu \end{Bmatrix} \tag{2.2}$$

and $\mathbf{F}$ is the vector of flux

$$\mathbf{F} = \begin{Bmatrix} uh \\ u^2 h + gh^2/2 \end{Bmatrix} \tag{2.3}$$

where h is the depth of the water column, u is the depth-averaged velocity, and $\mathbf{S}$ is the source term:

$$\mathbf{S} = \begin{bmatrix} 0 \\ -gh(S_0 + S_f) + Bgd^3\eta_{xxx} + 2Bgd^2\eta_{xx} \end{bmatrix} \tag{2.4}$$

where S_0 and S_f represent the bed slope and friction slope, respectively. B is the dispersion coefficient, which is chosen as 1/15 after (Borthwick, 2006). η is the wave elevation, $d = h - \eta$ is the still water level, and g is the gravitational acceleration. The following bed friction relationship is used to close the equations:

$$S_f = \frac{n^2 u|u|}{h^{4/3}} \tag{2.5}$$

where n is the Manning's roughness coefficient, and is taken to be 0.03 to account for the increase in effective roughness caused by the mobile bed.

The system of equations is solved using a Gudunov-type finite volume method (FVM). The numerical model without the dispersion terms has been validated against by analytical solutions by (Carrier et. al., 2003) and the experimental results by (Synolakis, 1987)).

2.2 Subsurface Pore Water Pressure Simulator - FEM

To investigate the sub-surface pore water pressure response due to wave loading, we employ a mixed finite element (FEM) formulation to simultaneously solve for the deformation of the solid matrix and pore-fluid pressures. The governing equations for the coupled model consist of balance equations enforcing the conservation of mass and linear momentum for the solid/fluid mixture (Biot 1941, Borja 2006), which may be expressed in local form as

$$\nabla \cdot (\sigma' - p\mathbf{1}) + \rho\mathbf{g} = \mathbf{0} \tag{2.6}$$

$$\nabla \cdot \frac{\partial \mathbf{u}}{\partial t} + \nabla \cdot \mathbf{v} + \frac{n}{K'}\frac{\partial p}{\partial t} = 0 \tag{2.7}$$

Here, σ' is the effective Cauchy stress, p is the pore water pressure, $\mathbf{1}$ is a unit symmetric tensor, ρ is the combined density of the solid/fluid mixture, $\mathbf{g}$ is a vector of gravity accelerations, $\mathbf{u}$ is the displacement of the solid matrix, $\mathbf{v}$ is the Darcy velocity, n is the porosity, and K' is the effective bulk modulus of the pore fluid. If the pore space is fully saturated, then the effective modulus is simply equal to the bulk modulus K_w of pure water (~2.2 GPa). Even a small amount of entrained air (i.e. near, but not complete, saturation) can lead to a drastic reduction in the effective modulus and a large increase in the apparent compressibility of the pore fluid (Yamamoto et al. 1978, Verruijt 1969).

We supplement the governing balance laws with constitutive relations for the solid and fluid components, as well as appropriate boundary conditions. We assume the effective stress follows a linear elastic constitutive law. For the pore fluid, we employ Darcy's Law. Key assumptions used in developing the above model are that (1)

the system remains isothermal, (2) both material and geometric nonlinearities may be ignored, (3) the compressibility of the solid skeleton is much greater than the intrinsic compressibility of the solid grains, (4) the porosity and permeability remain constant and are strain-independent, and (5) the domain of interest is close to full saturation.

The numerical implementation is based on the discrete variational form of the above equations (White and Borja 2008), in which the solid displacements, pressures, and seepage velocities are introduced as primitive variables ($\mathbf{u}/p/\mathbf{v}$ form).

3. VALIDATION STUDIES

3.1 Overview of Experimental Study

To study the dynamics of breaking solitary wave runup and drawdown over a fine sand beach, as well as the bed responses to transient waves loads, a set of large-scale laboratory experiments were conducted. The results are used to validate the numerical model. The experiments were carried out in the Tsunami Wave Basin at O.H. Hinsdale Wave Research Laboratory at Oregon State University in 2007. A 2D flume with dimensions 48.8 m × 2.16 m wide × 2.1 m deep was built for this experiment inside the 3D Tsunami Wave Basin. In the experiment study, breaking solitary waves with an initial height of 60 cm were generated over a flat concrete bottom with an initial water depth of 100 cm, which then propagated up onto a fine sand beach with a nominal profile of 1:15 constant slope. The sand had a median diameter D_{50} = 0.21 mm, and a uniformity coefficient Cu = D_{50}/D_{10} = 1.67. The initial bed profile for the 60 cm solitary wave, as shown in Figure 1, exhibited a slight S-shape, which is the result of many previous solitary waves of smaller amplitude. Details about the facilities, instruments, bed configurations, wave conditions, and experimental procedures were presented in Young & Xiao (2008a,b).

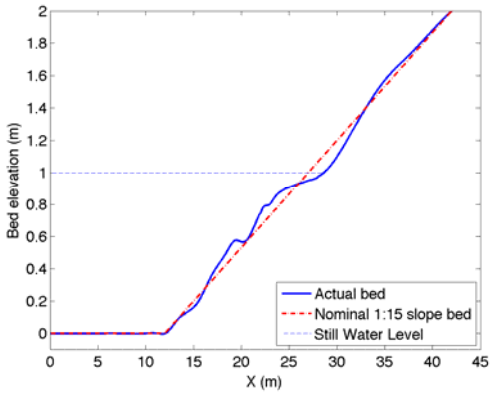

Figure 1. The nominal bed profile (1:15 constant slope) and the actual initial bed profile prior to the 60 cm solitary wave runs. The still water line is also indicated.

In the experiment, numerous sensors were deployed to measure the water surface elevation, flow velocity, sediment concentration, pore water pressure, and bed profile. In this paper, however, we will only present the measured time-histories from the wave gauge and pore water pressure sensors at the initial shoreline, x=27m. The locations of the sensors shown in this paper and the schematic of the wave flume are shown in Figure 2. The waves were generated by a piston wave maker at x=0m, as shown in Figure 2, and propagated towards the slope on the right.

3.2 Predicted vs. Measured Wave and Pore Pressure Time Histories

The region near the coastline is the area of focus because of its importance to coastal structure and coastal

ecology, and because that is the region most susceptible to wave-induced liquefaction failure. Therefore, we focus on the validation with experimental measurements obtained from sensors deployed right at the shoreline.

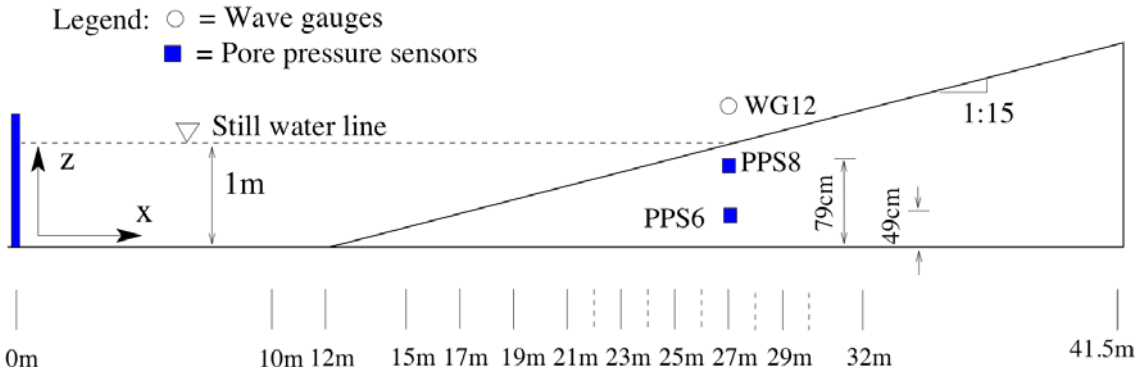

Figure 2. Elevation view of the experimental setup. The triangular area between 12m and 41.5m is the mobile (sand) bed, which sits on the concrete bottom of the flume.

Comparison of the measured and predicted time-histories of the surface water elevation at WG12 at x=27m is shown in Figure 3. The first peak is due to the arrival of the turbulent bore, which formed after the plunging breaker impinged on the shallow water at x~24m. The maximum runup occurred at x~38.5 m at t~13 sec, followed immediately by wave drawdown. The second peak in Figure 3 is due to the passing of the shallow water column during the wave drawdown. Notice the water dropped below the initial shoreline (i.e. wave height less than 0) for 15 sec < t < 30 sec due to the set down. Considering the complex wave breaking, bore formation and collapse processes, the overall agreement between the numerical predictions and experimental measurements is satisfactory. The agreement begins to deteriorate for t>20 sec due to complications introduced by wave-wave interactions, hydraulic jump and large re-circulating flow that occurred at the end of the wave drawdown.

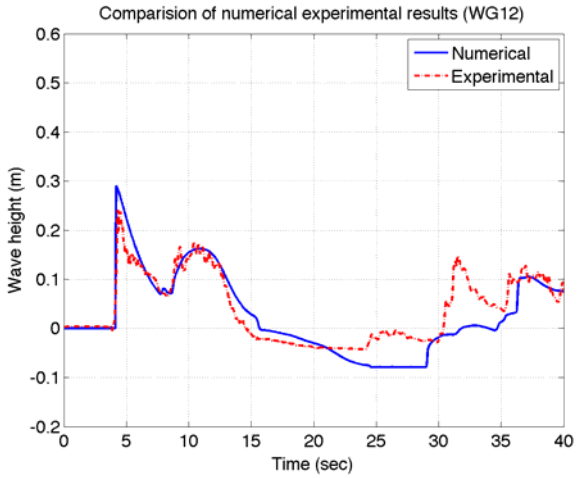

Figure 3. Comparison of numerical and experimental results of the wave elevation at x = 27 m.

Using the FVM wave simulator, a time-history of the hydrostatic pressure distribution at the bed surface was developed. This pressure history was then used as a boundary condition in the FEM pore pressure analysis. From the experimental setup (Figure 2), it is clear that portion of the sand bed above the still water line, or the vadose zone, is unsaturated. A preliminary analysis indicated that the fluid behavior within the vadose zone had only minor influence on the saturated region. Therefore, for the purposes of this analysis, only the region below the water table was modeled. The intrinsic permeability was assumed to be isotropic, with a spatially

constant value of 1.5 x 10^{-12} m^2. For the solid constitutive response, bulk modulus $K_d = 85$ MPa and Poisson ratio $\upsilon = 0.2$ were assumed. The effective modulus for the pore fluid was $K' = 4$ MPa.

Figure 4 presents time histories of the evolution of the change in pore pressure from the initial hydrostatic state at two representative points, PPS-6 and PPS-8 located 49 cm and 79 cm from the concrete bottom, respectively. In general, the prediction is quite good, particularly given the uncertainties in the spatial variation of the permeability field and in the compressibility of the pore fluid. The sudden rise in pore pressure at PPS-6 around 4 sec is attributed to the compression of the solid skeleton due to the arrival of the wave at the bed surface. A pure diffusion model does not capture this sudden rise---a key advantage of the coupled solid/fluid formulation. The first and second peaks correspond to the passing of the water column associated with wave runup and drawdown, respectively. Beyond 13 sec, the pressure agreement deteriorates, with the numerical simulations overestimating the pore pressures. Part of this disagreement can be attributed to small errors in the simulated wave profile. Note in Figure 3, for example, that the true wave height is slightly overestimated after 13 sec. The remaining disagreement is likely due to spatial variation of the porosity, saturation, and grain size due to cumulative wave action.

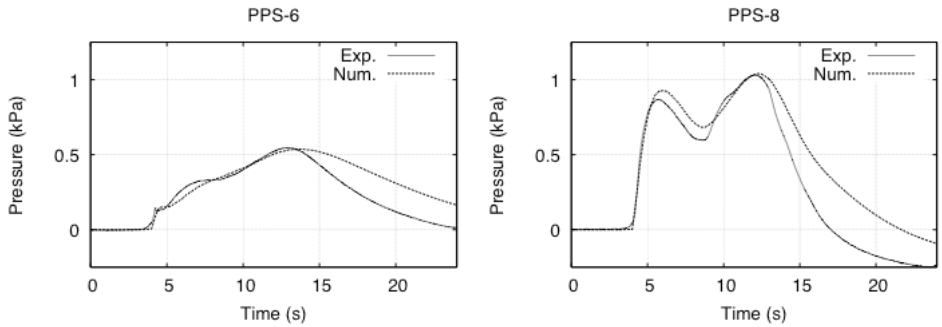

Figure 4. Comparison of experimental and numerical results for pore pressure at PPS-6 and PPS-8.

4. RESULTS

4.1 Overview of Model Setup

Numerical case studies are presented for a full-scale problem: a solitary wave with an initial height 10 m over an initial water depth of 20 m. The slope of the fine sand beach is selected to be 1:15 and 1:5 to represent a mild slope and a steep slope beach, respectively. The depth of the sand layer to impervious bed rook is assumed to be 20 m. The properties of the sand are assumed to be the same as mentioned in Section 3.

Wave and Pore Pressure Responses – 1:15 slope

The computed time-histories of the wave surface elevation at 3 locations near the initial shoreline for the 1:15 slope case are shown in the left pane of Figure 5. Snapshots of the wave profile during the drawdown are shown in the right pane of Figure 5. Notice that the wave broke prior to reaching the shoreline, and hence the maximum wave height at the shoreline (x=0 m) is only a little higher than 5 m. The maximum runup occurred at t = 49.4 sec with the maximum horizontal excursion at x = –233.2 m. After which, the drawdown begins. The influence of the drawdown can be discerned by the small change in slope of the water surface elevation at ~50 sec. At 25 m offshore, the water surface elevation dropped below zero for t>50 sec due to setdown. At 50 m offshore, a second hump between t=40-60 sec appeared due to the hydraulic jump that formed during the drawdown. The wave profiles in the right pane of Figure 5 shows that the setdown exposed a 50 m wide by 4 m deep area immediately below the initial shoreline.

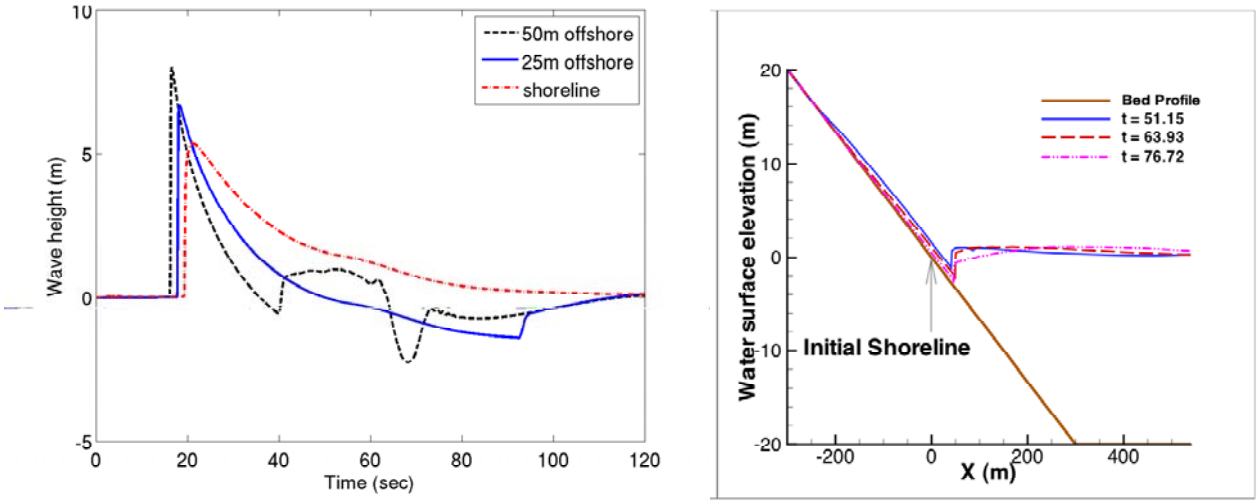

Figure 5. 10 m wave running onto a 1:15 slope bed. Left Pane: time series of wave height at three different locations. Right pane: sequences of wave profiles during the drawdown.

4.3 Wave and Pore Pressure Responses – 1:5 slope

The time-histories of the wave surface elevations and drawdown wave profiles for a 10-m solitary wave over a 1:5 slope are shown in Figures 6 in the same manner as in the 1:15 slope case above. Compared to the 1:15 case, there was no obvious wave shoaling and breaking due to the steep 1:5 slope. Another significant difference compared to the 1:15 slope case is that the duration of the runup and drawdown processes is much shorter because of the steeper slope. For the 1:5 slope, The maximum runup occurred at t = 24.2 sec with the maximum excursion to x = –139.8 m. The extent of the seepage face for the 1:5 slope is approximately 25 m wide by 5 m deep, which is narrower but wider than that in the 1:15 case.

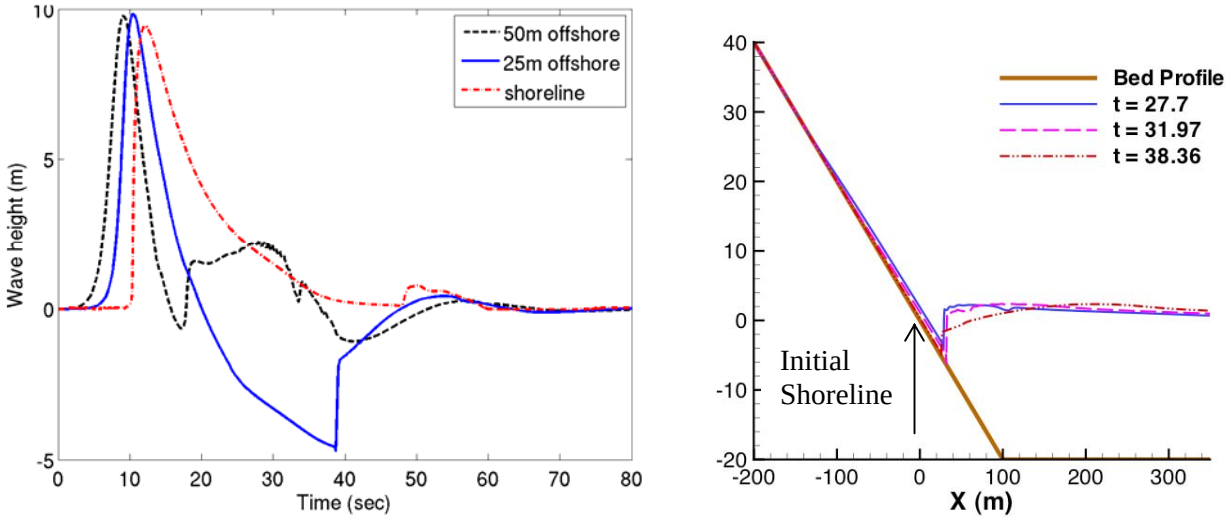

Figure 6. 10 m wave running onto a 1:5 slope bed. Left Pane: time series of wave height at three different locations. Right pane: sequences of wave profiles during the drawdown.

4.3 Pore Pressure Responses – 1:5 and 1:15 Slopes

Figure 7 presents the evolution of the excess pore pressure in the two beds during the runup and drawdown process. For each slope case, the pressure is sampled at four points at increasing depths (0.0m, -0.5m, -1.0m, and -1.5m). The horizontal position of the sampled cross-section is chosen to lie immediately in front of the

hydraulic jump that formed during the wave drawdown. At this point, the maximum drop in water level is observed, and this cross-section is thus considered critical in terms of liquefaction potential. The horizontal position of the hydraulic jump varies for the two cases, and so the pressures are sampled at points 25m from the initial shoreline in the 1:5 case, and 40m from the shoreline in the 1:15 case.

We observed that the rise and fall in the pore pressures in the 1:5 case occurred over a significantly shorter time span than the 1:15 case. Peak pressures are also larger. These observations are in keeping with the observed wave profiles for the two cases shown in the previous section. The interplay between diffusion and compression processes is also evident in the pore pressure time-histories, particularly at deeper depths. At even down to 1.5 m below the bed surface, for example, both slopes showed an instantaneous rise in pore pressures with the arrival of the wave. This rise is a result of the immediate compression of the solid skeleton due to the sudden increase in overburden stress caused by arrival of the wave. As time progresses, however, diffusive mechanisms begin to dominate.

Figure 8 presents an analysis of potential liquefaction zone for the 1:5 and 1:15 beds. The criterion used to determine the size of the liquefied zone is if the vertical hydraulic gradient drops below a threshold value of -0.6 m/m. It is interesting to note that although the rate of loading and unloading for the 1:5 slope is approximately twice as fast as the 1:15 slope, the extent of the zone at risk to liquefaction is very similar. In both cases, the high liquefaction potential zone extends horizontally for tens of meters, but the low permeability of the sand confines the at-risk zone to the top 1.5 m of depth.

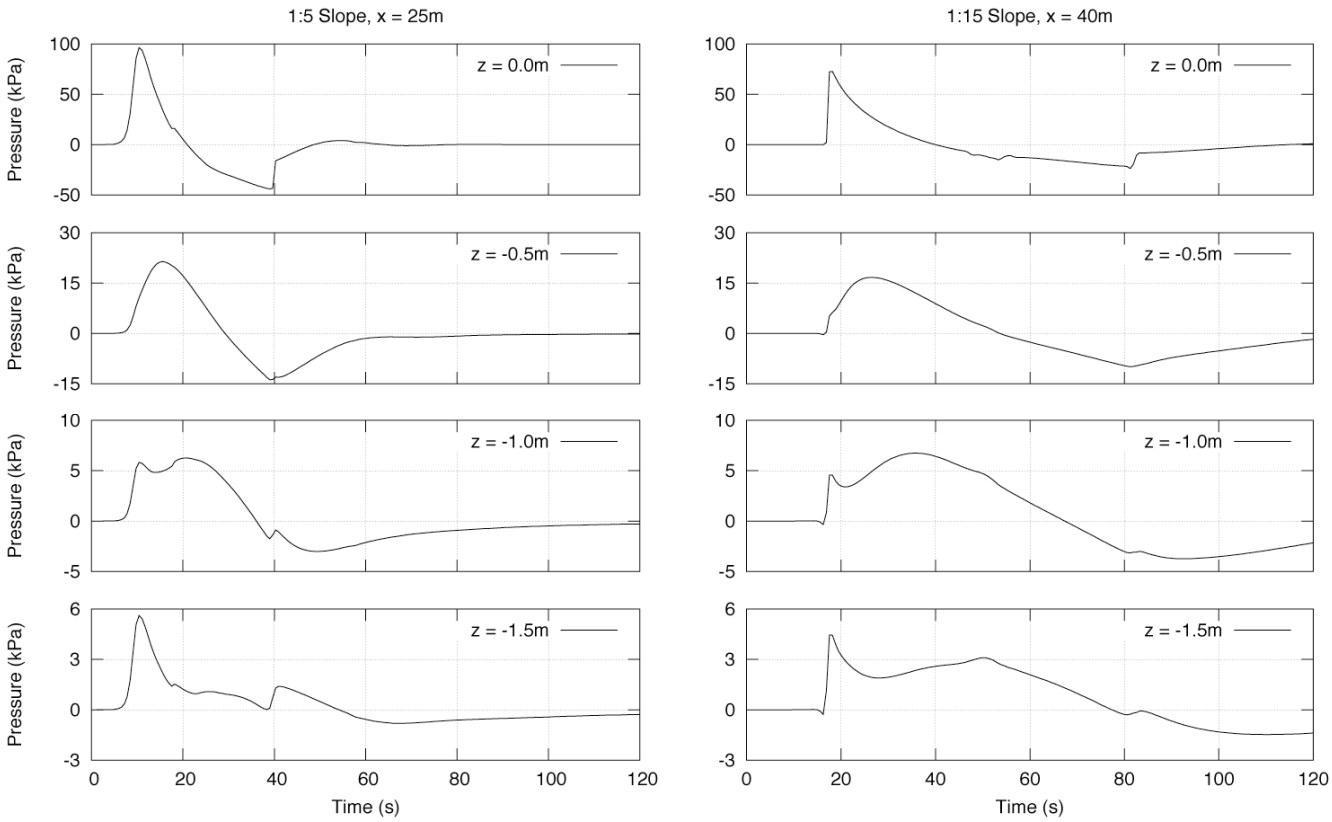

Figure 7. Time-evolution of the excess pore pressure (kPa) at increasing depths for the 1:5 and 1:15 slope cases (left and right column, respectively). In each case, pressures are measured along a vertical cross-section immediately in front of the position where the hydraulic jump forms in the receding wave.

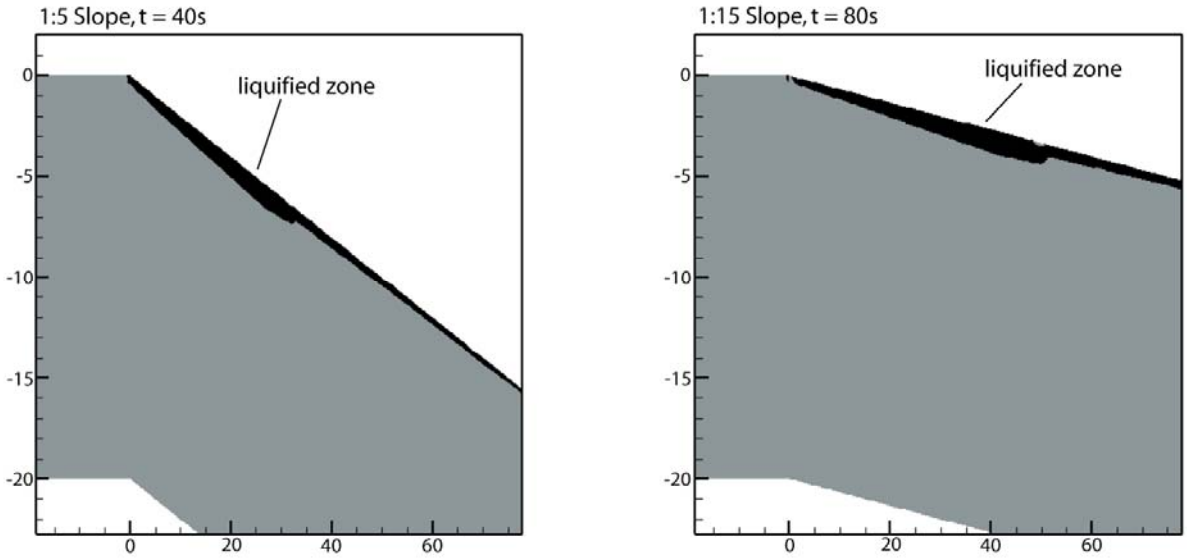

Figure 8. Spatial extent of potentially liquefied sand for the 1:5 and 1:15 slopes at two representative times. Liquefaction is assumed to occur when the hydraulic gradient is less than a threshold value of -0.6 m/m.

5. CONCLUSIONS

The objective of this work is to investigate the liquefaction potential of planar fine sand slopes during tsunami runup and drawdown. The transient pressure distribution acting on the slope due to wave runup and drawdown is computed by solving for the hybrid Boussinesq – nonlinear shallow water equations using a finite volume method (FVM). The subsurface pore water pressure distribution is solved simultaneously using a finite element method (FEM). The numerical methods are validated by comparing the results with experimental measurements from a large-scale laboratory study of breaking solitary waves over a planar fine sand beach. Numerical predictions are shown for a 10m solitary wave over a 1:15 and 1:5 sloped fine sand beach. The results show that the soil near the bed surface along the seepage face created during the drawdown is subject to liquefaction failure.

ACKNOLWEDGEMENT

The authors would like to acknowledge funding by the National Science Foundation through the NSF George E. Brown, Jr. Network for Earthquake Engineering Simulation (grant no. 0530759) and through the NSF CMMI grant no. 0653772. The first author would also like to acknowledge the financial support through the UPS visiting professor program at Stanford, and the third author would like to acknowledge the support through the NSF Graduate Research Fellowship Program.

REFERENCES

Bennett, R.H. (1978). Pore-water pressure measurements: Mississippi Delta submarine sediments. *Mar. Geotech.*, 2, 177-189.
Bennett, R.H. and Faris, J.R. (1979). Ambient and dynamic pore pressures in finegrained submarine sediments: Mississippi. *Applied Ocean Research*, 1:3, 115-123.
Biot, M. A. (1941). General theory of three-dimensional consolidation. *J. Appl. Phys.* ***12*****:2** 155–164.

Borja, R. (2006). On the mechanical energy and effective stress in saturated and unsaturated porous continua. *Int. J. of Solids and Structures*, **43:6** 1764–1786.
Borthwick, A.G.L, Ford, M., Weston B.P., Taylor, P.H., and Stansby, P.K.,(2006). *Proceedings of the Institution of Civil Engineers, Maritime Engineering*, **159:MA3,** 97–105.
Carrier, G.F., Wu, T.T., and Yeh, H. (2003). "Tsunami run-up and draw-down on a plane beach" *J. Fluid Mech.*, **475**, 79-99.
Chowdhury, B., Dasari, G.R., Nogami, T. (2006). Laboratory study of liquefaction due to wave-seabed interaction. *Journal of Geotechnical and Geoenvironmental Engineering*, **132:7**, 842-851.
Demars, K.R. and Vanover, E.A. (1985). Measurements of wave-induced pressures and stresses in a sand bed, *Mar. Geotech*., **6:1**, 29-59
Jeng, D.S. (2003). Wave-induced sea floor dynamics, *Appl. Mech. Review*, **56:4**: 407-429.
Jha, B., and Juanes, R (2007). A locally conservative finite element framework for the simulation of coupled flow and reservoir geomechanics. *Acta Geotechnica* ***2*:3** 139–153.
Kim, D.H., Cho, Y.S., and Kim, W.G. (2004). "Weighted averaged flux-type scheme for shallow water equations with fractional step method" *J. of Engrg. Mech*., **130:2**, 152-160.
Kudella, M., Oumeraci, H., de Groot, M.B., and Meijers, P. (2006). Large-scale experiments on pore pressure generation underneath a Caisson Breakwater, *J. waterway, port, coast. ocean eng.*, **132:4**, 310-324.
Liu, P., Yeh, H., Synolakis, C., and Shuto, N. (2004). "*The third international workshop on long-wave runup models*." MUD history, < http://www.cee.cornell.edu/longwave> (Sept. 17, 2006)
Maeno, Y.H. and Hasegawa, T. (1987). In-situ measurements of wave-induced pore pressure for predicting properties of seabed deposits, *Coastal Engineering of Japan*, 30:1, 99-115.
Okusa, S. (1985). Measurements of wave-induced pore pressure in submarine sediments under various marine conditions, *Mar. Geotech*., **6:2**, 119-144.
Okusa, S., and Uchida, A. (1980). Pore-water pressure change in submarine sediments due to waves, *Mar. Geotech*., 4:2 145-161.
Okusa, S., Nakamura, T., and Fukue M. (1983). Measurements of wave-induced pore pressure and coefficients of permeability of submarine sediments during reversing flow, *Seabed Mechanics*, B Denness (ed), Graham and Trotman Ltd, London, 113-122.
Phillips, R. and Sekiguchi, H. (1992). Generation of water wave trains in drum centrifuge, *Proceedings of International Symposium on Technology in Ocean Engineering*, **1**, 29-34.
Sassa, S. and Sekiguchi, H. (1999). Wave-induced liquefaction of beds of sands in a centrifuge, *Géotechnique*, 49:5, 621-638.
Sekiguchi H. and Phillips, R. (1991). Generation of water waves in a drum centrifuge. *Proceedings of International Conference on Centrifuge*, 343-350
Sleath, J.F.A. (1970). Wave-induced pressures in beds of sand, *Journal of Hydraulics, Div. ASCE*, **96:2,** 367-378.
Synolakis, C. E. (1987). "The runup of solitary waves." *J. Fluid Mech*. **185**, 523-545.
Tonkin, S., Yeh, H., Kato, F., and Sato, S. (2003). Tsunami scour around a cylinder, *J. Fluid Mech., **496***, 165-192.
Toro, E.F. (2000). Shock-capturing methods for free-surface shallow flows, Wiley, New York.
Tsui, Y.T. and Helfrich, S.C. (1983). Wave-induced pore pressures in submerged sand layer, *J. of Geotechnical Engineering, Div. ASCE*, **109:4**, 603-618..
Tzang, S.Y. (1992). Water wave-induced soil fluidization in a cohesionless fine-grained seabed, PhD Dissertation, University of California, Berkeley
Verruijt, A. (1969). Elastic storage of aquifers. In *Flow Through Porous Media* (ed. R.J.M. Dewiest). Academic Press.
Wei, Y., Mao, X.Z., and Cheung, K.F. (2006). "Well-Balanced Finite-Volume Model for Long Wave Runup" *J. of Waterw., Port, Coastal, and Ocean Eng.*, **132:2**, 114-124.
White, J., and Borja, R (2008). Stabilized low-order finite elements for coupled solid-deformation / fluid-diffusion and their application to fault zone transients. *Comp. Meth. Appl. Mech. Eng. doi:10.1016/j.cma.2008.05.01*.
Yamamoto, T., Koning, H.L., Sellmeijer, H., and van Hijum, E. (1978). On the response of a poro-elastic bed to

water waves. *J. Fluid Mech.* **87 :1**, 193-206.
Yeh, H., Kato, F., and Sato, S. (2001). Tsunami scour mechanisms around a cylinder, Tsunami Research at the end of a critical decade, G.T. Hebenstreit (ed), Kluwer Academic Publishers, Netherlands, pp. 33-46.
Young, Y.L. and Xiao, H (2008). Enhanced Sediment Transport due to Wave-Soil Interactions, Proceedings of 2008 NSF Engineering Research and Innovation Conference, Knoxville, TE, January 8-10, 2008.
Young, Y., and Xiao, H. (2008). Erosion and deposition processes due to solitary waves over a movable bed, Tech. Rep. 0803, Department of Civil and Environmental Engineering, Princeton University.
Zen, K. and Yamazaki, H. (1990). Mechanism of wave-induced liquefaction and densification in seabed. *Soils and Foundations*, **30:4,** 90-104.
Zen, K. and Yamazaki, H. (1991). Field observation and analysis of wave-induced liquefaction in seabed, *Soils and Foundations*, 31:4, 161-179.
Zhang, J.E. (1996). “Run-up of ocean waves on beaches.” California Institute of Technology, Pasadena, California.
Zoppou, C. and Roberts, S. (2000). Numerical solution of the two-dimensional unsteady dam break. *App. Math. Modelling*, **24**, 457-475.